Journal of The Electrochemical Society, **149** (8) C423-C428 (2002)
0013-4651/2002/149(8)/C423/6/$7.00 © The Electrochemical Society, Inc.

Superconformal Electrodeposition of Silver in Submicrometer Features

T. P. Moffat,*,z B. Baker,* D. Wheeler, J. E. Bonevich, M. Edelstein, D. R. Kelly, L. Gan, G. R. Stafford,* P. J. Chen, W. F. Egelhoff, and D. Josell

National Institute of Standards and Technology, Gaithersburg, Maryland 20899, USA

The generality of the curvature-enhanced accelerator coverage (CEAC) model of superconformal electrodeposition is demonstrated through application to superconformal filling of fine trenches during silver deposition from a selenium-catalyzed silver cyanide electrolyte. The CEAC mechanism involves (*i*) increase of local metal deposition rate with increasing coverage of a catalytic species adsorbed on the metal/electrolyte interface and (*ii*) significant change of local coverage of catalyst (and thus local deposition rate) in submicrometer features through the changing area of the metal/electrolyte interface. Electrochemical and X-ray photoelectron experiments with planar electrodes (substrates) are used to identify the catalyst and obtain all kinetic parameters required for the simulations of trench filling. In accord with the model, the electrolyte yields optically shiny, dense films, hysteretic current-voltage curves, and rising current-time transients. Experimental silver deposition in trenches from 350 down to 200 nm wide are presented and compared with simulations based on the CEAC mechanism. All kinetics for the modeling of trench filling come from the studies on planar substrates. The results support the CEAC mechanism as a quantitative formalism for exploring morphological evolution during film growth.
 [DOI: 10.1149/1.1490357]

Manuscript submitted November 26, 2001; revised manuscript received February 8, 2002. Available electronically June 21, 2002.

Superconformal electrodeposition of copper in the Damascene process for microelectronic fabrication is enabling a new generation of integrated circuits. The use of copper interconnections has permitted faster clock speeds, enhanced reliability, and lower processing cost. Central to the success of the electrodeposition process is its ability to yield void and seam-free filling of high aspect ratio features. Empirically, such superfilling of trenches and vias with copper results from more rapid metal deposition (growth) at the bottom of the feature than at the sidewalls. Early models of superfilling of copper in trenches assumed location-dependent growth rates derived from diffusion-limited accumulation of only an inhibiting species.[1,2] Such models were unable to predict several key experimental observations.[3-6] Understanding of the superfill phenomena has improved substantially in the past two years. Electrolytes for the study of superconformal electrodeposition of copper have been fully disclosed.[6,7] A correlation between efficacy for superconformal filling of fine features, hysteresis in cyclic current-voltage studies, and recrystallization of deposits has also been demonstrated.[6] In addition, the curvature-enhanced accelerator coverage (CEAC) mechanism has been used to quantitatively predict superconformal copper deposition in trenches.[8-11] and vias[12] by electrodeposition as well as by surfactant-catalyzed chemical vapor deposition (CVD).[13,14]

The CEAC mechanism involves the gradual accumulation of a metal-deposition-rate-accelerating species at the surface of the growing metal. If there is a deposition-rate-inhibiting species, it is presumed to be weakly bound and displaced, or altered, by the catalyst. Superfill can occur without an inhibiting species (see Ref. 13, 14) but only if adsorption of the catalyst leads to significantly faster deposition than occurs in its absence. All adsorbed species are presumed to remain on or float at the metal/electrolyte interface during deposition (consistent with more recent work that has explicitly quantified the effect of potential dependent additive consumption[15]). Thus, local compression (or expansion) of adsorbed accelerator occurs with the reduction (or increase) of surface area that accompanies growth at points of high positive (or negative) curvature. Models based on the CEAC mechanism have been shown to yield predictions that agree well with experimental results for superconformal electrodeposition of copper over a wide range of processing conditions. This includes a period of conformal growth, bottom-up filling or void formation, and creation of overfill bumps, for filling of trenches between approximately 350 and 100 nm wide and 500 nm deep.[8-11]

The CEAC mechanism as described is quite generic. Indeed, as noted above, it has recently been used to explain superconformal filling of fine features by iodine-catalyzed CVD of copper. Similarly, there is no fundamental reason that superconformal filling by electrodeposition should be limited to either copper or acid sulfate based chemistries. This paper therefore examines the link between superconformal silver filling of fine features on patterned substrates and hysteresis during current-voltage studies on planar substrates. The catalyst in the additive-containing silver-cyanide electrolyte that was used for these studies was identified using X-ray photoelectron spectroscopy (XPS). This paper presents two principal results: (*i*) it predicts superfilling conditions using only a CEAC-based model with all kinetic parameters obtained from current-voltage and current-time studies of deposition on flat electrodes, and (*ii*) it demonstrates superconformal filling of trenches in the electrolyte under conditions consistent with the predictions. While the electrical resistivity of bulk silver is only slightly lower than that of bulk copper at room temperature, the effective electrical resistivity of silver in fine features like narrow lines has been noted to be substantially less than that of similar copper lines due to surface scattering effects.[16]

Experimental

Details for chemical studies of planar specimens.— Electrodeposition on freshly polished silver electrodes was examined in a commercial plating bath (Techni-Silver E, Lot no. f-3-0388 and F-1-11-4049, both from Technic, Inc.[a]) that are stated to contain 0.34 mol/L $KAg(CN)_2$ and 2.3 mol/L KCN and two additional proprietary components, a surfactant (*i.e.*, wetting agent) and a brightener or catalyst. Electrochemical experiments were performed using a standard cell with three silver electrodes serving as the reference, counter, and working electrodes, respectively. (All potentials are referenced to the immersed Ag wire and thus are cited as overpotentials. The open-circuit potential corresponds to −0.670 V *vs.* the saturated calomel electrode.) The silver working electrode was polished with a 320 grade SiC paper immediately before each experiment. The electrode was then masked with electroplater's tape (3M[a]) leaving an exposed electrode area of 0.97 cm^2. The deposition reaction was examined through cyclic current-voltage (i-η) experiments initiated from the open-circuit, or reversible, potential, swept to a

* Electrochemical Society Active Member.
z E-mail: thomas.moffat@nist.gov

[a] Product names are included only for accuracy of experimental description. They do not imply NIST endorsement.

particular negative overpotential and then swept back. Deposition was also investigated through studies of current-time transient $i(t)$ experiments at constant voltage performed over a similar range of potentials.

The evolution of the chemistry of the growth interface was examined by XPS. For these experiments, 100 nm thick electron beam evaporated copper films on silicon were used as substrates. Silver was deposited at -0.35 V for various periods of time in the electrolyte. Upon emersion, the electrodes were rinsed with water and transferred to ultrahigh vacuum (UHV) within 30 min. Binding energy data were referenced to internal copper and gold standards and the values are reported relative to Cu $(2p_{3/2}) = 932.7$ eV, Cu $(3p_{3/2}) = 75.1$ eV, and Au $(4f_{7/2}) = 84.0$ eV.

Details for filling studies with patterned specimens.—The superfilling capacity of the electrolyte was examined by electroplating silver in submicrometer trenches at different overpotentials. Specimens for the filling studies were fabricated as follows. Electron beam lithography was used to pattern trenches into polymethylmethacrylate that had been spin-coated on silicon substrates. All trenches were ≈0.41 μm deep, with widths from 350 to 200 nm, corresponding to aspect ratios (height/width) from ≈1.2 to 2. Each specimen consisted of six groups of ≈100 μm long trench arrays, with each array consisting of parallel trenches, including one of each aspect ratio. A silver seed layer was deposited by electron beam evaporation immediately prior to electrodeposition. Further details on the patterning and seed layer deposition process can be found elsewhere.[6] A relatively thick 130 nm seed was used in an attempt to reduce electrolyte-induced damage of the patterned poly(methyl methacrylate (PMMA) substrate; this corresponds to coverage of ≈10 nm on the sidewalls of the trenches. Nonetheless, pinholes or voids in the seed layer often resulted in distortion of the underlying PMMA resist due to reaction with the alkaline electrolyte. Interpretation of images is subject to this concern.

Following electrodeposition, the patterned wafers were cross sectioned and mechanically polished to 0.5 μm grit. Residual polishing damage was removed from the specimen surfaces using an argon ion flux prior to imaging on a field-emission scanning electron microscope (SEM). A subset of specimens was also prepared for imaging by transmission electron microscope (TEM).

Studies with Planar Substrates

Kinetics of the deposition reaction experiments on planar substrates.—An example of the i-η characteristics of the additive-containing electrolyte is shown in Fig. 1. The solid curve was acquired at the 1 mV/s sweep rate. Individual data points extracted from $i(t)$ data curves obtained at the indicated voltages are also included. Hysteretic behavior is clearly evident in the cyclic i-η curve (a much smaller hysteresis loop observed with an additive-free electrolyte not shown here is associated with increasing surface area as the associated deposits were optically rough). Because electrodeposits produced in the additive-containing electrolyte were dense and near specular in nature, the hysteresis visible in Fig. 1 is not caused by changing surface area. Rather, it reflects actual acceleration of the deposition rate caused by accumulation of a catalytic species on the surface during the cycle (note that this conclusion is supported by the results in Fig. 2c where the current density, after increasing steadily, saturates at a value close to that on the return sweep of the i-η curve at the same voltage, *i.e.*, the $t = 1200$ s, $\eta = -0.35$ V data point on Fig. 1). The current densities observed in the $i(t)$ experiments at $t = 20$ s, as recorded on Fig. 1, reflect deposition on a still uncatalyzed metal surface in the additive-containing electrolyte as they lie quite close to the curve obtained during cyclic current-voltage studies in an additive-free solution (not shown).

Examination by XPS of electrodeposited films grown at -0.35 V for 1000 s revealed the accumulation of selenium, or some derivative thereof, on the surface as shown in Fig. 2a. High resolution spectra reveal the selenium $L_3M_{45}M_{45}$ Auger line is at 177.7 eV

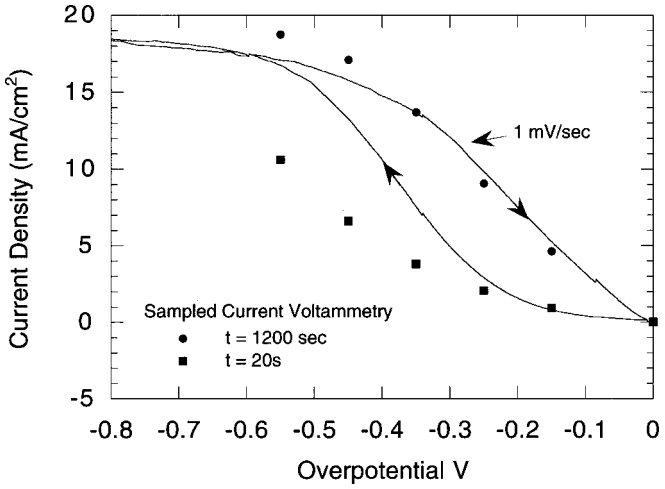

Figure 1. A cyclic current-voltage study of the additive-containing electrolyte reveals hysteretic behavior. Sweep rate was 1 mV/s. Similar behavior is also evident in the voltage dependence of the sampled current density data (data points at 20 and 1200 s taken directly from $i(t)$ studies in Fig. 4). The 1200 s data, which corresponds to saturated or fully catalyzed behavior, is seen to be consistent with the return sweep of the i-η curve. The 20 s data is taken as a measure of the deposition rate for an uncatalyzed surface.

while the Ag $(3d_{5/2})$ photoelectron peak is at 368.1 eV, suggesting the formation of silver selenide at the interface. The accumulation of selenium during silver deposition is shown in Fig. 2b. The ratios of the time-dependent integrated intensities of the selenium $L_3M_{45}M_{45}$ Auger and the Ag $(3d_{5/2})$ photoelectron peaks are plotted with the current transient data in Fig. 2c. There is a clear correlation between the silver deposition rate (*i.e.*, current density) and the selenium coverage. The saturation selenium coverage is estimated to be ≈0.3 to 0.4 of a monolayer relative to a clean silver surface. [This value was derived by taking the sensitivity factor for the Se $L_3M_{45}M_{45}$ to be 1.29 relative to 2.25 for the Ag $(3d_{5/2})$, the values taken or derived from standard spectra in Ref. 19 and a 1.5 nm escape depth for the Ag $(3d_{5/2})$, given its ≈1188 eV kinetic energy.]

It is well known that cyanide is strongly adsorbed on the silver electrode and that reduction of silver cyanide complexes is a kinetically slow process involving the formation-decomposition of an adsorbed complex.[17,18] The results in Fig. 2 indicate that selenium acts as an effective catalyst for the reduction of such complexes. This might occur either through displacement or disruption of the adsorbed cyanide or silver cyanide complex that forms in its absence.

Cyclic i-η sweeps for several sweep ranges are summarized in Fig. 3a. Fits to the data, derivation of which is discussed later, are shown in Fig. 3b. A switching potential below -0.4 V yields saturation prior to completion of the return sweep at ≈800 s. This is consistent with the time constant that characterizes the $i(t)$ data shown in Fig. 4a. Simulations of the $i(t)$ data, using the same kinetics used to model the i-η data in Fig. 3, are shown in Fig. 4b (and also discussed later). The saturation evident in Fig. 3a and 4a was also apparent when cyclic i-η sweeps were conducted multiple times; current densities on both the outward and return sweeps essentially traced the return sweep established during the first cycle (not shown).

Kinetics of the deposition reaction—Modeling experiments with planar substrates.—The electrochemical experiments for selenium-catalyzed silver deposition can be simulated using the CEAC model. The i-η and $i(t)$ data in Fig. 3a and 4a, respectively, are modeled using the generalized reversible current-overpotential equation

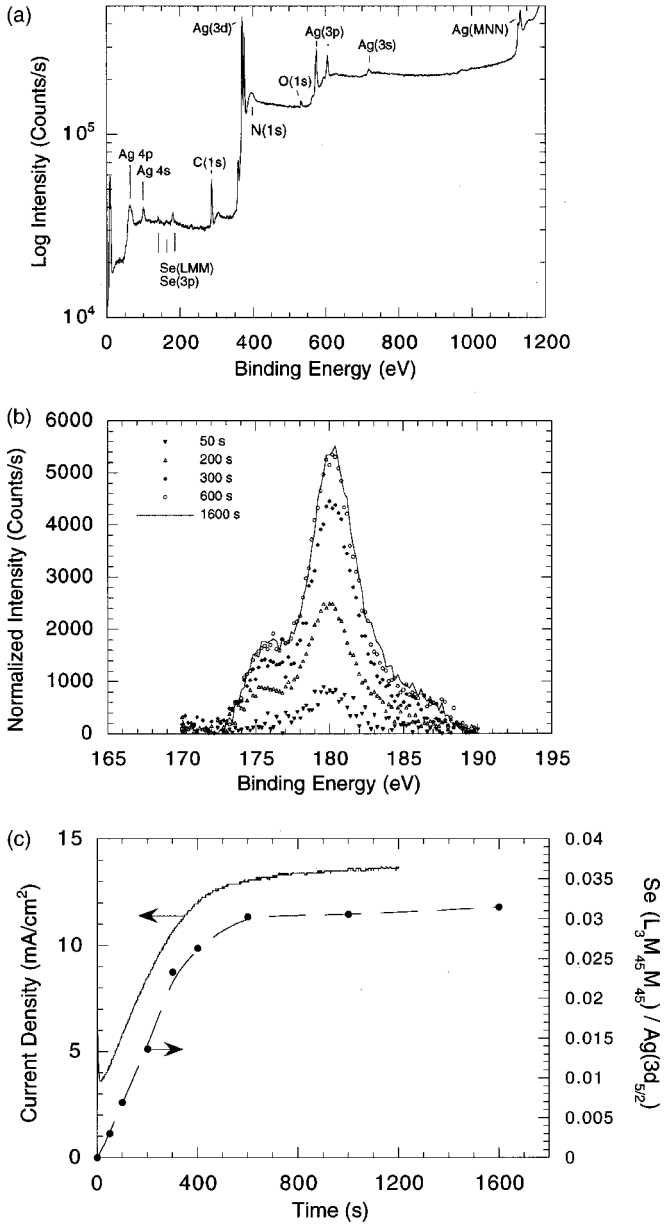

Figure 2. (a) A survey spectrum for a sample after 1000 s of silver deposition at −0.35 V. (b) The selenium $L_3M_{45}M_{45}$ Auger signal as a function of deposition time. The intensities are scaled by the areas under the associated Ag $(3d_{5/2})$ photoelectron peaks. (c) The correlation between acceleration of the deposition rate and accumulation of the selenium catalyst on the silver surface is apparent for deposition at −0.35 V. The XPS data are delineated as solid circles with the dashed line being only a guide to the eye.

$$i(\theta,\eta) = i_o(\theta)\left(1 - \frac{i}{i_L}\right)\left[\exp\left(-\frac{\alpha(\theta)F}{RT}\ \eta\right) - \exp\left(\frac{(1-\alpha(\theta))F}{RT}\ \eta\right)\right] \quad [1]$$

The term $(1 - i/i_L)$ equals the ratio of the silver ion concentration at the interface relative to the bulk concentration (*i.e.*, C^i_{Ag}/C_{Ag}) reflecting the concentration gradient across the boundary layer. This deviates from unity at large overpotentials. The exchange current density $i_o(\theta)$ and the transfer coefficient $\alpha(\theta)$ are modeled as linearly dependent on the normalized surface coverage of the catalyst θ, defined in terms of the maximum coverage Γ. The transport-limited deposition rate, $i_L \approx 18$ mA/cm^2, is determined by diffusion across the boundary layer (thickness δ), free convection, and silver ion concentration in the bulk electrolyte according to the relationship $i_L = FD_{Ag}C_{Ag}/\delta$. A diffusion coefficient of $D_{Ag} = 7.6 \times 10^{-6}$ cm^2/s was calculated based on a boundary layer thickness $\delta = 135$ μm and $C_{Ag} = 3.4 \times 10^{-4}$ mol/cm^3 (the latter specified by the electrolyte manufacturer). Note that $F = 96485$ C/mol, $R = 8.314$ J/mol K, and $T = 293$ K.

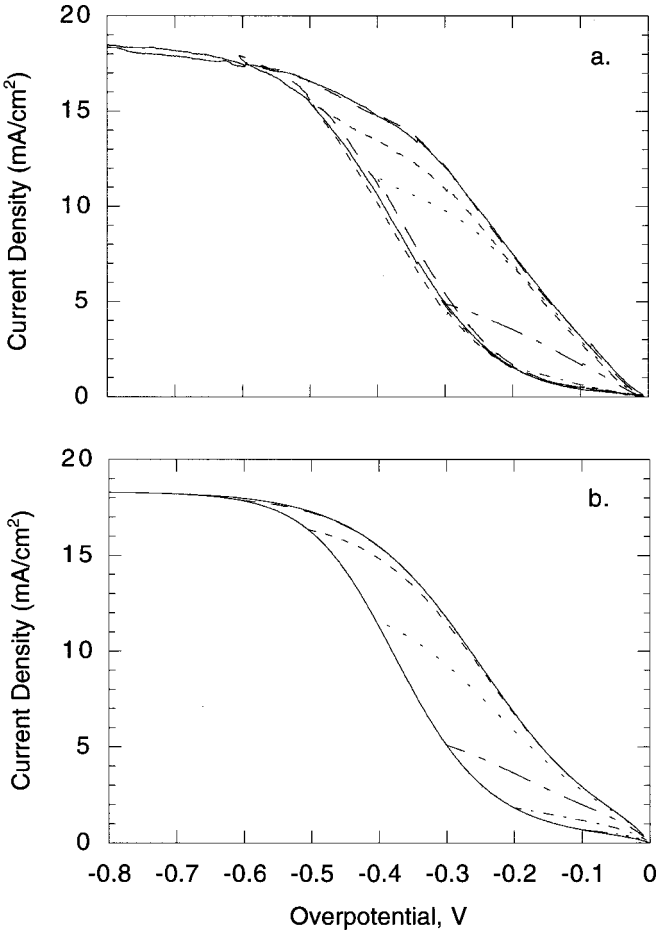

Figure 3. (a) Slow sweep cyclic current-voltage studies of deposition on planar substrates reveal hysteresis that increases with the voltage sweep range. Note the saturation on the return sweeps for larger sweep range. Sweep rate 1 mV/s. (b) Simulations obtained using kinetic parameters optimized to simultaneously fit both i-η data in Fig. 3a and $i(t)$ data in Fig. 4a.

The selenium catalyst is assumed to adsorb according to Langmuir kinetics

$$\frac{d\theta}{dt} = k' C^i_{Se}(1 - \theta) \quad [2]$$

In Eq. 2, k' gives the kinetics of selenium accumulation onto the metal surface for selenium concentration in the adjacent electrolyte C^i_{Se}. This concentration is related to the bulk concentration C_{Se} by equating the adsorbing selenium flux to that diffusing across the boundary layer

$$k' C^i_{Se}(1 - \theta) = \frac{D_{Se}}{\Gamma}\frac{(C_{Se} - C^i_{Se})}{\delta} \quad [3]$$

where Γ is the saturation coverage of the catalyst. Using Eq. 2 and 3 it can be shown that the parameters D_{Se}, δ, and Γ affect catalyst accumulation only through the ratio $D_{Se}/\delta\Gamma$. For diffusion-limited

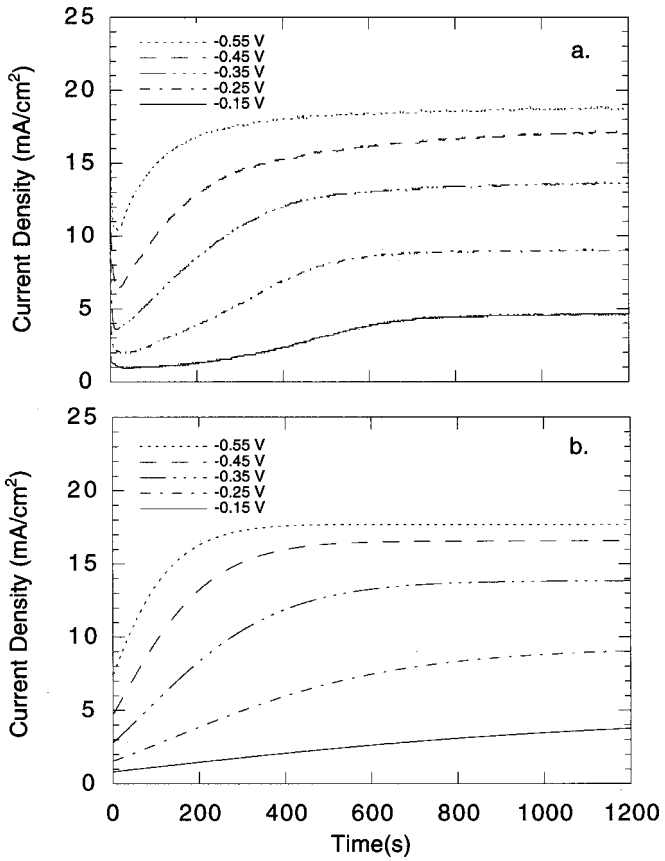

Figure 4. (a) Current-time studies of deposition on planar substrates at different overpotentials. Current-densities at 20 and 1200 s were used in Fig. 1. (b) Simulations obtained using kinetic parameters optimized to simultaneously fit both i-η data in Fig. 3a and $i(t)$ data in Fig. 4a.

accumulation ($D_{Se}/\delta\Gamma \ll k'$), the time constant for accumulation scales with $\delta\Gamma/C_{Se}D_{Se}$. For accumulation limited by interface kinetics ($D_{Se}/\delta\Gamma \gg k'$), the time constant for accumulation scales with $1/k'C_{Se}$. The time constant obtained by fitting the experimental data when either of these limiting conditions dominates, thus specifies only the value of the appropriate product, not the values of the individual parameters D_{Se}, C_{Se}, δ, or Γ. This is particularly significant in the present work where C_{Se} is not known due to commercial proprietary restrictions. Accordingly, kinetic parameters consistent with the data in Fig. 1 have been determined by fixing $C_{Se} = 1 \times 10^{-8}$ mol/cm^3, and $\Gamma = 7.6 \times 10^{-10}$ mol/cm^2, the latter corresponding to a 0.33 site occupancy on Ag(111). The diffusion coefficient D_{Se} and interface kinetics $k'(\eta)$ are permitted to vary in the optimization. The fixed values C_{Se} and Γ, though expected to individually be of the correct order of magnitude,[6] are not necessarily correct. They are fixed only to limit the parameter space for data fitting to the most relevant parameters. Data where crossover conditions ($D_{Se}/\delta\Gamma \approx k'$) dominate would be better fit by adjusting all parameters. However, it is unlikely that a substantially more meaningful picture would be obtained due to the resulting large number of fitting parameters, the quality of the data, and the simplicity of the model (which neglects consumption). Similarly, the value of D_{Se} obtained will only be as correct, individually, as the other parameters. The functional form of the interface kinetics $k'(\eta)$ obtained, though scaled by a constant, should more closely reflect the true voltage dependence, being the only voltage dependent quantity.

Using Eq. 3 to eliminate C^i_{Se}, Eq. 2 can be numerically integrated to obtain $\theta\,[t, D_{Se}, k'(\eta)]$ for the experimental conditions used to obtain each of the i-η and $i(t)$ data curves shown in Fig. 3a and 4a. Using the functional forms of θ thus obtained, $k'(\eta)$, $i_o(\theta)$, $\alpha(\theta)$, and D_{Se} were obtained by optimizing the fit of the curves predicted by Eq. 1 to the data. In fitting the i-η data, the adsorption rate constant k', which was found to increase with overpotential, is held at its maximum value for the entire return sweep to model obstruction of any inhibiting layer's healing by the adsorbed catalyst. The kinetic parameters thus obtained are $k'(\eta) = 5.2 \times 10^4 + 5.1 \times 10^6 \quad \eta^2$ (cm^3/mols), $i_o(\theta) = 0.32 + 0.86\theta$ (mA/cm^2), and $\alpha(\theta) = 0.17 + 0.11\theta$. Inclusion of a term proportional to η^2 for the interface kinetics was found to give a slightly better fit than inclusion of a term proportional to either η or η^3. The diffusion coefficient of the catalyst that optimizes the fit to the data is $D_{Se} = 4.5 \times 10^{-6}$ cm^2/s. Figures 3b and 4b show the fits to the data in Fig. 3a and 4a, respectively, obtained with these kinetic parameters. The root-mean-square deviation between the data and the fits is 0.5 mA/cm^2, quite small considering that data from two different types of experiments, including thirteen curves, eight of them cyclic, and all having inflections, have been fit with just seven parameters. Note that the fitting parameters just obtained from these studies on planar substrates fully define the kinetics that are used in the modeling of trench filling that follows.

Studies with Patterned Substrates

Filling of trenches-modeling.—In the CEAC model describing deposition on patterned (more generally, nonplanar) substrates, Eq. 1 describing the evolution of surface coverage of catalyst on the surface of a flat substrate is modified to

$$\frac{d\theta}{dt} = \frac{i\Omega_{Ag}}{F}\,\kappa\theta + k'C^i_{Se}(1-\theta) \qquad [4]$$

The first term on the right reflects the change of the local coverage θ due to changing surface area. This term is proportional to the local interface velocity, v, equal to $i(\theta,\eta)\Omega_{Ag}/F$ ($\Omega_{Ag} = 10.3$ cm^3/mol), and the local curvature κ of the interface. The κ dependence leads to increasing (decreasing) local coverage on concave (convex) surfaces during growth. This term dominates at the bottoms of superfilling features. In computational modeling based on this equation, where area reduction would have led to catalyst coverage exceeding unity, the additional catalyst was deleted to keep the coverage at unity. This is equivalent to either presuming local incorporation of the catalyst within the metal deposit or desorption or deactivation of a molecule that is no longer deposition-rate-enhancing. Simulations of trench filling in the selenium catalyzed electrolyte involved an explicit solution of the diffusion equations that govern silver and catalyst transport through the electrolyte to the evolving surface of the filling trench as well as boundary conditions appropriate for the local catalyst coverage. A code using the level-set method for interface tracking, with all kinetics from the studies conducted on planar substrates, was implemented. Further details can be found elsewhere.[10]

The feature filling predictions are shown in Fig. 5. Superconformal growth is achieved when the catalyst coverage, while still low on the sidewalls, becomes concentrated on the bottom of the trench by area reduction, resulting in bottom-up filling in Fig. 5a and e-k. If the aspect ratio of the trench is too great, or the associated variation of deposition rate along the surface profile too small, the sidewalls impinge before the bottom of the trench can escape (Fig. 5b-d and 1), creating a vertical seam or void in the center of the trench. The transition between superfilling and seam formation is predicted to be a function of potential with the fill/fail boundary, *i.e.*, the highest aspect ratio trench that can be filled without seam formation, moving from an aspect ratio of $\approx$1 at $\eta = -0.15$ V to an aspect ratio as high as $\approx$2.25 at $\eta = -0.48$ V and then back down to $\approx$2 at $\eta = -0.69$ V. It should be noted that there is no reason to believe that these are the highest aspect ratio features that can be filled from this electrolyte system, as it is unlikely that this composition is optimized for superconformal deposition. A slight canting of the

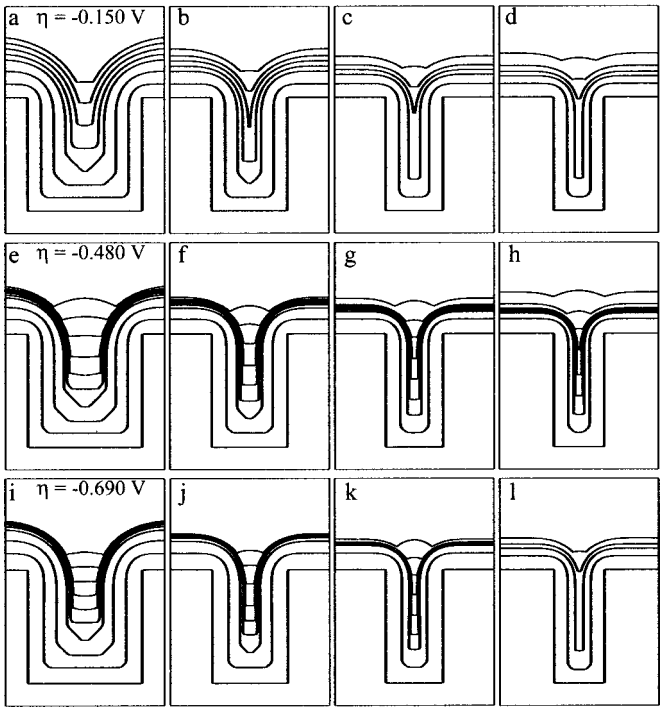

Figure 5. Simulations of silver deposition in trenches with aspect ratios of 1.0, 1.5, 2.0, and 2.25 (left to right) for indicated overpotentials. All simulations are for trenches 0.5 μm deep. Trenches are predicted to fill superconformally for aspect ratios up to, and including, 1 at −0.15 V, 2.25 at −0.48 V, and 2 at −0.69 V. Insufficient differentiation of deposition rate on the bottom and sidewalls is predicted to result in seam formation in b, c, d, and 1.

trench sidewalls, such that the trenches are wider at the top than at the bottom, will enable geometric leveling that will increase the nominal aspect ratio of the features that can be filled robustly.[6,20]

Filling of trenches-experiments.—Silver deposition into trenches 0.41 μm deep and between approximately 350 and 200 nm in width was examined using the selenium-catalyzed electrolyte. As shown in Fig. 6, filling improves as η goes from −0.375 to −0.480 V, with trenches of aspect ratios up to 1 or 1.5 filling at the lower voltage (Fig. 6b and a, respectively) and trenches with aspect ratio up to 1.5 and 2 filling at the latter (Fig. 6d and c, respectively). The highest

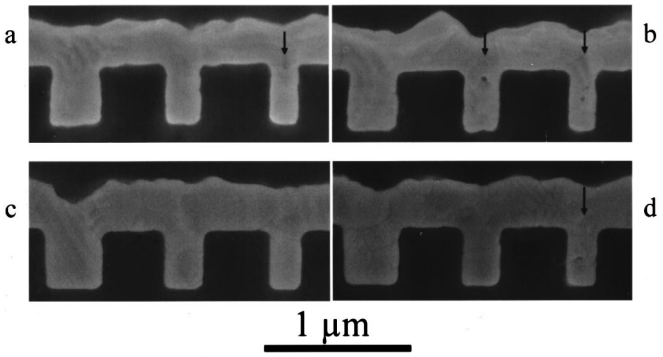

Figure 6. SEM images of trenches filled at overpotentials η: (a and b) −0.375 V and (c and d) −0.480 V. Trenches from two groups, showing filling behavior representative of that observed in all six groups on each specimen, are shown from each specimen. Aspect ratios of the features are approximately 1.1, 1.5, and 2 from left to right in each of the four groups shown. Arrows indicate the trenches that contain voids.

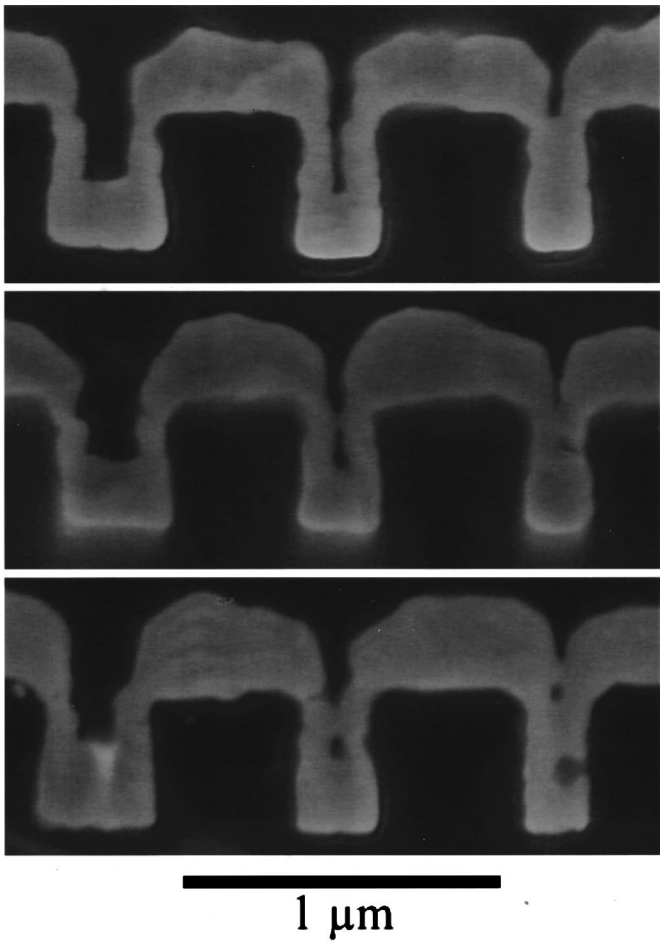

Figure 7. SEM images of trenches filled at overpotential η = −0.325 V (top to bottom). The formation of voids in the finer features is not consistent. The variability is likely associated with the visible roughness of the surface. All three groups come from the same specimen.

aspect ratios that fill at these two overpotentials, both in value and trend with overpotential, are consistent with the predictions in Fig. 5.

It should be noted that when η was increased to −0.585 and −0.69 V, voids formed even at the tops of the trench with aspect ratio of 1 (not shown). This contrasts with the simulations, where filling is predicted for aspect ratios up to 2 over this voltage range. These unexpected voids are believed to be related to the roughness of the impinging side wall deposits (Fig. 7). The roughness of the metal deposits is due, in part, to the roughness of the lithographically defined sidewalls (see Fig. 7) caused by attack in the alkaline electrolyte. Additional roughening at the larger overpotentials is likely associated with the operation at the current limit (see Fig. 3). These conclusions are supported by the fact that surface roughness was much reduced, and no voids were formed during filling of vias patterned in "hard" oxides/nitrides, that were not attacked by the electrolyte.[21] Further work will be required in order to address the impact of roughness evolution on feature filling.

Close examination of the largest feature imaged in Fig. 6c reveals grain contrast; parallel twin boundaries pass diagonally across the trench indicating that a single grain spans its cross section. As this area originally included a polycrystalline seed layer, this is unlikely to have formed during the growth process. This suggests that a postdeposition recrystallization process has occurred analogous to that reported for electrodeposited copper films. The effect is more clearly revealed in the TEM micrograph of a cross sectioned speci-

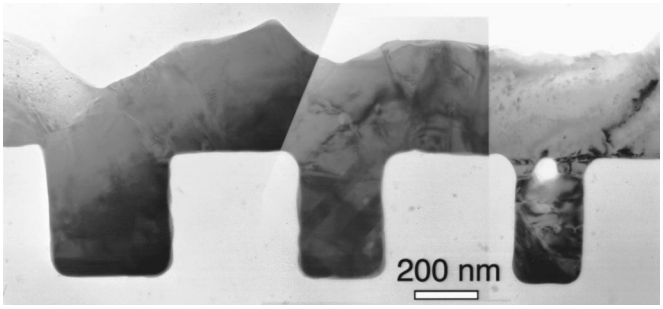

Figure 8. Montaged TEM images of trenches filled at overpotential $\eta = -0.480$ V. The twins across the central feature indicate there is no seam, clearly demonstrating the superconformal filling of the trench with silver.

men in Fig. 8. Of particular significance are the large grains, including twins, that fill the two larger trenches.

Recrystallization

The spontaneous recrystallization of copper at room temperature is a key attribute in the successful implementation of copper electrodeposition in Damascene processing because it results in a substantial decrease (~20%) of the electrical resistivity. If silver deposits do in fact recrystallize, they offer the prospect of a slightly lower resistivity. The electrical resistances of unpatterned silver deposits from the selenium catalyzed electrolyte were measured using a conventional four-point probe in order to examine this matter in more detail. The silver films were grown galvanostatically at 10 mA/cm^2 to a thickness of 1 μm. The substrates were comprised of a 100 nm thick copper seed-layer supported on silicon (100) wafers with a 2.5 nm thick chromium adhesion layer. Following silver deposition the films were rinsed with water and transferred to the probe station within a few minutes, and the resistance was monitored for a period of up to 8 days.

Measurements begun within minutes of film deposition revealed a total decrease in resistance of ~1.8% over two days. Continued monitoring over the following six days revealed no further change. This resistance drop is much smaller than that associated with recrystallization of copper films, and seemingly inconsistent with the large grains evident in Fig. 6 and 8. Because specimen preparation for cross sectioned specimens involved heating the specimens to cure the supporting epoxy layer, resistance measurements were also made both before and after annealing specimens in flowing argon at 150°C for 30 min. The annealed specimens exhibited a resistance drop of ≈10%, similar in size to the resistivity drops exhibited by recrystallizing copper films.[6] This implies that recrystallization of the silver specimens occurs during preparation of cross-sectioned SEM and TEM specimens, and can be induced by very modest annealing temperatures.

Discussion and Conclusion

The curvature-enhanced accelerator coverage (CEAC) model has been extended to describe superconformal electrodeposition of silver from an electrolyte containing a selenium catalyst or brightener. Features with aspect ratios larger than 0.5 (height/width) were seen to be filled during silver electrodeposition (Fig. 6 and 8), the definition of superconformal filling. Catalyst accumulation at the metal/electrolyte interface affects the silver deposition kinetics, enhancing the silver deposition rate, and manifesting as hysteretic current-voltage curves and rising current transients in studies on planar substrates. The accumulation of the catalyst was shown to lead to enhancement of the silver deposition rate. As given by Eq. 1, the enhancement of the deposition rate expressed as $v(\theta = 1)/v(\theta = 0)$ is rather small. Ignoring silver ion depletion effects, it goes from approximately 6 to 14 as the overpotential η goes from -0.1 to -0.3 V at room temperature. This contrasts with the behavior observed for copper electroplating where rate enhancements ranging from 30 to 300 are possible.[8-11] This is manifest in the much smaller hysteresis for cyclic current-voltage studies with silver (Fig. 3a) as compared to that exhibited in similar experiments with copper[8,9] and void-free filling of lower aspect ratio features than are achievable with copper. Both of these observations are predicted quantitatively by the CEAC model. Experiments examining the filling of 350-200 nm wide trenches were compared with shape-change simulations based on the CEAC mechanism. With all kinetics used for modeling of feature filling obtained from the experiments on planar substrates, experimental and modeling results for trench filling were found to be in reasonable agreement. The generality of the CEAC model has thus been demonstrated by extension to a chemical system that is distinct from that originally used to develop the physical model.

It is noteworthy that the CEAC mechanism also offers a quantitative formalism for understanding the morphological evolution of an arbitrary surface profile and thus explains the widely known brightening action evoked by selenium addition to silver cyanide electrolytes.

References

1. P. C. Andricacos, C. Uzoh, J. O. Dukovic, J. Horkans, and H. Deligianni, *IBM J. Res. Dev.*, **42**, 567 (1998).
2. A. C. West, *J. Electrochem. Soc.*, **147**, 227 (2000).
3. J. Reid and S. Mayer, in *Advanced Metallization Conference 1999*, p. 53, M. E. Gross, T. Gessner, N. Kobayashi, and Y. Yasuda, Editors, MRS, Warrendale, PA (2000).
4. T. Ritzdorf, D. Fulton, and L. Chen, in *Advanced Metallization Conference 1999*, p. 101, M. E. Gross, T. Gessner, N. Kobayashi, and Y. Yasuda, Editors, MRS, Warrendale, PA (2000).
5. E. Richard, I. Vervoort, S. H. Brongersma, H. Bender, G. Beyer, R. Palmans, S. Lagrange, and K. Maex, in *Advanced Metallization Conference 1999*, p. 149, M. E. Gross, T. Gessner, N. Kobayashi, and Y. Yasuda, Editors, MRS, Warrendale, PA (2000).
6. T. P. Moffat, J. E. Bonevich, W. H. Huber, A. Stanishevsky, D. R. Kelly, G. R. Stafford, and D. Josell, *J. Electrochem. Soc.*, **147**, 4524 (2000).
7. P. Taephaisitphongse, Y. Cao, and A. C. West, *J. Electrochem. Soc.*, **148**, C492 (2001).
8. T. P. Moffat, D. Wheeler, W. H. Huber, and D. Josell, *Electrochem. Solid-State Lett.*, **4**, C26 (2001).
9. D. Josell, D. Wheeler, W. H. Huber, and T. P. Moffat, *Phys. Rev. Lett.*, **87**, 016102 (2001).
10. D. Wheeler, D. Josell, and T. Moffat, Submitted.
11. D. Josell, D. Wheeler, W. H. Huber, J. E. Bonevich, and T. P. Moffat, *J. Electrochem. Soc.*, **148**, C767 (2001).
12. D. Josell, D. Wheeler, and T. P. Moffat, *Electrochem. Solid-State Lett.*, **5**, C49 (2002).
13. D. Josell, D. Wheeler, and T. P. Moffat, *Electrochem. Solid-State Lett.*, **5**, C44 (2002).
14. D. Josell, D. Wheeler, and T. P. Moffat, in *Advanced Metallization Conference 2001*, A. J. McKerrow, Y. Shacham-Diamand, S. Zaima, and T. Ohba, Editors, p. 363, MRS, Warrendale, PA (2002).
15. T. P. Moffat, D. Wheeler, and D. Josell, Unpublished work.
16. M. Hauder, J. Gstottner, W. Hansch, and D. Schmitt-Landsiedel, *Appl. Phys. Lett.*, **78**, 838 (2001).
17. R. Y. Bek and N. A. Rogozhnikov, *J. Electroanal. Chem.*, **447**, 109 (1998).
18. H. Baltruschat and W. Vielstich, *J. Electroanal. Chem.*, **154**, 141 (1983).
19. *Handbook of X-Ray Photoelectron Spectroscopy*, C. D. Wagner, W. H. Rigg, L. E. Davis, J. F. Moulder, and G. E. Muilenberg, Editors, Perkin Elmer Corp., Physical Electronics Division, Eden Prairie, MN (1978).
20. D. Varadarajan, C. Y. Lee, A. Krishnamoorthy, D. J. Duquette, and W. N. Gill, *J. Electrochem. Soc.*, **147**, 3382 (2000).
21. D. Josell, B. Baker, C. Witt, D. Wheeler, and T. P. Moffat, *J. Electrochem. Soc.*, Submitted.